engineering proceedings

MDPI

Proceeding Paper

Thermomechanical Fatigue Behaviour Monitoring of Additively Manufactured AISI 316L via Temperature Harmonic Analysis †

Mattia Tornabene [1], Danilo D'Andrea [2], Francesco Willen Panella [3], Riccardo Penna [3], Giacomo Risitano [2] and Giuseppe Pitarresi [1,*]

[1] Dipartimento di Ingegneria, University of Palermo, Viale delle Scienze, 90128 Palermo, Italy; mattia.tornabene@unipa.it
[2] Department of Engineering, University of Messina, Contrada di Dio (S. Agata), 98166 Messina, Italy; giacomo.risitano@unime.it (G.R.)
[3] Dipartimento di Ingegneria dell'Innovazione, University of Salento, 73100 Monteroni di Lecce, Italy; francesco.panella@unisal.it (F.W.P.)
* Correspondence: giuseppe.pitarresi@unipa.it
† Presented at the 54th Conference of the Italian Scientific Society of Mechanical Engineering Design (AIAS 2025), Florence, Italy, 3–6 September 2025.

Abstract

Laser-based Powder Bed Fusion (LPBF) enables the fabrication of complex metal components but often results in high porosity and microdefect densities, compromising fatigue performance despite acceptable static properties. Standard fatigue characterisation methods are time-consuming and costly and yield scattered results due to defect-induced brittleness and residual stresses. This study investigates the application of thermographic techniques as a rapid alternative for evaluating the intrinsic fatigue behaviour of tensile coupons fabricated by LPBF employing AISI 316L steel. By monitoring surface temperature during stepwise static monotone and fatigue loading, thermographic methods aim to detect early hints of heat dissipation associated with microdamage initiation. Approaches based on temperature harmonic analysis have been implemented, allowing near-real-time and full-field mapping of stress distribution and damage development. Results show that harmonic metrics correlate with the material state and effectively track the thermoelastic effect-induced temperature changes. Some evidence is found regarding the onset of intrinsic heat dissipation, which needs to be confirmed by more focused and extensive experimental tests.

Keywords: thermoelastic stress analysis; infrared thermography; additive manufacturing; intrinsic dissipation; fatigue behaviour; energy methods

Academic Editors: Nicola Bonora, Umberto Galietti, Luigi Bruno, Davide Castagnetti, Cristiana Del Prete, Mario Guagliano and Vigilio Fontanari

Published: 21 April 2026

1. Introduction

Additive manufacturing (AM) technologies have gained increasing relevance in the production of metallic components for structural applications, enabling the creation of complex geometries and efficient material utilisation [1,2]. However, AM processes inherently generate specific micro-structural features such as local anisotropies, porosity, and solidification defects that can significantly affect the mechanical behaviour and fatigue performance of metallic alloys. Optimisation of fatigue behaviour in such materials remains a critical challenge that requires adequate and more efficient characterisation methodologies. Conventional fatigue testing procedures are often resource- and time-intensive. It is therefore relevant to investigate the adoption of faster and innovative approaches. In

recent decades, the development of the *Fatigue Limit Thermographic Method* (FLTM) has emerged as a convenient full-field monitoring technique, capable of rapidly providing indications of the intrinsic fatigue threshold of materials [3–5]. The method, commonly implemented via the stepwise procedure, consists of applying sinusoidal cyclic loading blocks of increasing amplitude and processing the resulting thermal response to extract intrinsic dispersion-related metrics. The evolution of these metrics may enable the identification of a critical stress threshold beyond which the thermal signatures associated with irreversible dissipation and damage initiation become evident.

The fatigue behaviour of metal additive-manufactured parts has often resulted in highly scattered data and significantly reduced fatigue lives. This is mainly due to the inherent higher porosity left by Laser Powder Bed Fusion (LPBF) processes. The presence of such microscale discontinuities may accelerate the formation of local cracks, whose threshold stress intensity factor range may be smaller than an intrinsic fatigue limit (i.e., that associated with a smooth, crack-free specimen), thus leading to a premature brittle fracture. This circumstance is, for instance, well represented by the Kitagawa–Takahashi (K-T) diagram defining a boundary for infinite fatigue life [6,7]. The intrinsic dissipation threshold sought by FLTMs is generally detected after a relatively small number of fatigue cycles and is associated with the onset of micro-damage and local micro-plasticity, at a stage when fatigue cracks are likely still too small to lead to critical failure.
Under the above premises, FLTMs may enable two significant advantages when applied to AM materials:

- Enable the measurement of an intrinsic fatigue threshold (equivalent to an endurance limit for zero crack size of K-T like failure envelope);
- Provide a rapid tool to assist the fatigue characterisation and allow a fatigue-driven AM process optimisation.

The adoption of FLTMs to study the fatigue behaviour of AM materials is still at an early evaluation stage, with only a few recent works yet available in the literature. These have generally employed classic FLTM approaches, based on measurement of surface temperature evolution, to detect the onset of intrinsic dissipation on AM AISI 316L [8–10], LPBF 304L SS [11], AM ALSI10Mg [12–14], and also thermoplastic composites [15]. The so-called FLTM static method, based on determining the temperature evolution along the elasto-plastic transition of a quasi-static tensile test, has also been adopted to AM AISI 316L [8,9]. TSA has also been used as a full-field technique to monitor the onset of long cracks in a CuAl9Ni5Fe4 bronze–aluminum built by Wire & Arc AM [16].

A limitation of conventional FLTM approaches, based on absolute temperature metrics, is their sensitivity to environmental effects such as convection, radiation, and reflections [17]. In the present work, a harmonic analysis of the thermal signal (TH) is instead carried out, allowing isolating frequency-modulated components that are less affected by environmental disturbances and more closely related to the *Thermoelastic Effects* reversible temperature changes [18]. Four harmonics-based metrics are used for the FLTM stepwise testing scheme: the amplitude and phase of the so-called first and second harmonics, i.e., the temperature harmonics at the loading frequency and twice the loading frequency. Each of these metrics has the potential to produce a signature at the onset of intrinsic dissipation, through various mechanisms reviewed in some recent papers [18–21].

The present work implements the TH-FLTM approach to AISI 316L tensile samples produced by LPBF-DMLS. The data presented refer to sinusoidal cyclic tensile tests performed with a load ratio R = 0.1, carried out in two different laboratories using the same step-wise protocol and samples coming from the same batch of production. Preliminary results of an ongoing experimental campaign are here commented, highlighting the potentials of the TH-FLTM approach in the evaluation of AM AISI 316L fatigue behaviour.

https://doi.org/10.3390/engproc2026131033

2. Materials and Methods

The following subsections describe the thermographic metrics used in the fatigue stepwise test, the material and related fabrication details, and the experimental setup and plan of experiments carried out.

2.1. Thermomechanical Model and Thermographic Metrics

The thermo-mechanical model considers a tensile specimen undergoing sinusoidal cyclic loading. A mono-axial stress field is assumed upon the coupon central gauge area, and the material exhibits a linear-elastic response. The loading frequency is sufficiently high to enable an adiabatic and reversible temperature change induced by the thermoelastic effect, here considered as the main thermo-mechanical heat coupling source. If no other heat exchanges with the environment are enabled, then the temperature change can be predicted by the second-order thermoelastic effect theory [18,22], written as

$$\Delta T = -T_o(K_o - K_1\sigma_m)\sigma_a \sin(\omega t) + T_o|K_2|(\sigma_a)^2 \cos(2\omega t) \quad (1)$$

where the thermoelastic coefficients are defined as

$$K_0 = \frac{\alpha}{\rho C_\varepsilon}; \quad K_1 = \frac{1}{\rho C_\varepsilon}\frac{1}{E^2}\frac{\partial E}{\partial T}; \quad K_2 = \frac{1}{\rho C_\varepsilon}\frac{1}{4E^2}\frac{\partial E}{\partial T}$$

From Equation (1), it is seen that a loading sine wave (with angular frequency ω) provides a thermoelastic response at the load frequency ω and at twice this loading frequency, 2ω. The temperature change can then be thought of as modulated by these two harmonics and can be written as

$$\Delta T(t) = A_\omega \sin(\omega t + \phi_\omega) + A_{2\omega} \sin(2\omega t + \phi_{2\omega}), \quad \omega = 2\pi f_L. \quad (2)$$

The above equation (2) implies that the temperature acquired while the material is cyclically loaded has two peculiar thermoelastic harmonics at ω and 2ω. The amplitude and phase of each of these two harmonics can be retrieved by sampling the temperature signal at a sufficiently high rate and using frequency domain filtering techniques such as the discrete Fourier transform or the least squares fitting [23].

In a stepwise test, as the stress amplitude σ_a increases, the amplitude and phase of the first and second thermoelastic harmonics are expected to increase/change. The onset of fatigue-damage-related heat dissipation has the potential to modify the rate of change of thermoelastic metrics, thus producing a signature of the onset of such dissipation at specific values of σ_a.

The mechanisms rendering each thermoelastic metric sensitive to heat dissipation may be different and are hereafter briefly reviewed.

- **First-Harmonic amplitude**: $A_\omega = E = T_o[K_o - K_1\sigma_m]\sigma_a$ (3)

An anomalous change in increase rate of T_o can then affect E. Moreover, the same material changes leading to dissipation might also induce changes in the thermoelastic constants (K_o in particular, since K_1 is generally negligible for steels) [18].

- **First-Harmonic phase**: $\phi_\omega = PhE \rightarrow -\sin(\omega t)$ (4)

https://doi.org/10.3390/engproc2026131033

PhE is 180°-shifted (i.e., $-sin(\omega t)$) from the load wave ($sin(\omega t)$). Some authors have postulated a slight shift from 180° due to the onset of visco-elastic delays between the load and the deformation [24], activated/exacerbated by heat dissipation.

- Second-Harmonic amplitude: $A_{2\omega} = D = |K_2|T_o{\sigma_a}^2$ (5)

The above equation represents the thermoelastic second-harmonic response. Similarly to E, D is also linearly sensitive to changes in T_o and to potential dissipation-induced changes in the material through K_2. Interestingly, D also increases with the square of the stress amplitude σ_a. Therefore, a non-linear trend in D is an expected thermoelastic response that should not be confused with a dissipation-induced change. Moreover, it may also happen that the load is not a pure sinusoid, containing a second-harmonic spurious component. This second-harmonic load harmonic would then produce a thermoelastic signal at 2ω, affecting the value of D [25].

- Second-Harmonic phase: $\phi_{2_\omega} = PhD \rightarrow \cos(2\omega t)$ (6)

The thermoelastic second-harmonic *PhD* has a specific time shift with respect to a pure sine load wave. If the latter is expressed as a $sin(\omega t)$, then from (1), it comes out that *PhD* has a time modulation given by $cos(2\omega t)$. This relative shifting between the load, and hence E, and *PhD* can be experimentally verified to ascertain that the second-harmonic response adheres to the thermoelastic model of (1) and whether a spurious second harmonic load might influence this expected prediction.

Several authors have linked the second-harmonic of temperature to heat-dissipation also through a non-thermoelastic mechanism [21,24,26,27]. More precisely, they have suggested that during a loading period, the activation of heat dissipation is usually triggered near the peaks and troughs of the load wave. This periodic heating results in a modification of the temperature modulation, characterised by a pronounced second-harmonic component. This component may be distinguished from the thermoelastic one by adding a suffix d. Therefore, the dissipative second harmonic D_d is expected to exhibit an increasing trend with σ_a after the onset of heat dissipation, and its phase is such that it aligns the peaks with the peaks and troughs of the thermoelastic first-harmonic of the load or temperature. This latter feature provides a criterion to ascertain if the nature of the measured second-harmonic is thermoelastic or dissipative, by comparing the relative shift between the measured first- and second-harmonic phases [18,25]. In light of the above, a dissipative second-harmonic temperature change would then have the following shape:

- Dissipative Second-Harmonic: $\Delta T_{d-2\omega} = -\cos(2\omega t) \cdot |D_d|$ (7)

2.2. Materials

The material analysed is **AISI 316L stainless steel**, produced by DMLS, which is an LPBF additive manufacturing technique. The specimen geometry adopted for both monotonic tensile and fatigue testing was designed in accordance with the *ASTM E466 standard* guidelines [28]. Each specimen had a length of 110 mm, a thickness of 4 mm, a gauge area width of 18 mm, and a gauge length of about 20 mm (see Figure 1). Manufacturing was commissioned to *MadeInAdd* S.r.L. and followed a refill/refresh strategy based on recycled feedstock. With reference to the Cartesian coordinates in Figure 1, the build-direction was aligned with the x-axis and the scanning orientation with the z-axis. A standard heat treatment was also executed by the manufacturer, whose details cannot be disclosed here in

this paper. The heat-treated samples were eventually post-processed to ensure dimensional tolerances below 0.1 mm and a surface roughness within the range 0.8–1.6 μm R_a.

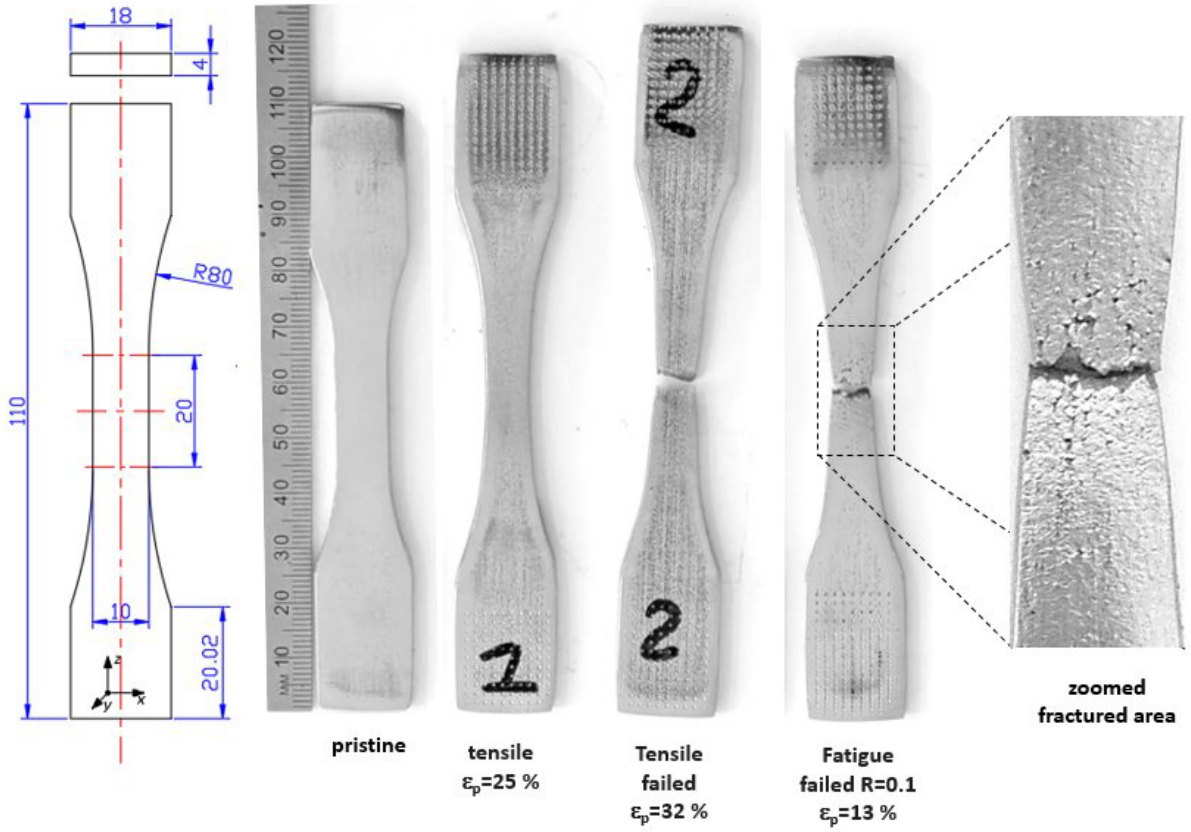

Figure 1. Samples geometry. From left to right: sample drawing, untested sample, sample after fatigue failure, sample after a tensile loading stopped before failure (about 25% of plastic deformation), and sample after tensile failure (deformation at failure of about 32%).

2.3. Plan of Experiments and Experimental Setup

Testing comprised uniaxial quasi-static tensile tests and stepwise fatigue tests at a load ratio $R = 0.1$. The stepwise tests presented here are performed on two samples taken from the same production/post-processing batch and tested in two different laboratories at the University of Palermo (UniPa) and Salento (UniSal) to acquire indications about the reproducibility of the methodology. Both laboratories adopted a stepwise increase in the stress amplitude $\Delta\sigma$ from 153 to 270 MPa over 14 steps ($1 \rightarrow 14$), with a loading frequency of 7.2 Hz (see Tables 1 and 2). Each load step of the UniPA and UniSal tests lasted, respectively, 2000 and 3000 cycles, and the acquired windows for the harmonic analysis generally comprised between 10 s and 30 s. It is noticed that for the sample test at UniPa, two windows were acquired for each step, one after 1000 cycles from the step start and one at around 1800 cycles. Both laboratories used FLIR cooled sensor cameras, with UniPa setting a sampling frequency of 81 Hz and UniSal of 150 Hz. The UniPa test also measured the central gauge uniaxial strain by means of a 25 mm extensometer.

Table 1. Plan of experiments UniPA.

UniPA		
LF 7.2 Hz & SF 81 Hz		
Steps	**$\Delta\sigma$[MPa]**	**Cycles**
1	153	2000
2	162	2000
3	171	2000
4	180	2000
5	189	2000
6	198	2000
7	207	2000
8	216	2000
9	225	2000
10	234	2000
11	243	2000
12	252	2000
13	261	2000
14	270	2000

Table 2. Plan of experiments UniSal.

UniSal		
LF 7.2 Hz & SF 150 Hz		
Steps	**$\Delta\sigma$[MPa]**	**Cycles**
1	153	3000
2	162	3000
3	171	3000
4	180	3000
5	189	3000
6	198	3000
7	207	3000
8	216	3000
9	225	3000
10	234	3000
11	243	3000
12	252	3000
13	261	3000
14	270	3000

3. Results

Results are presented separately in two subsections: one regarding the static thermographic method, applied on the thermal data acquired alongside the static tensile tests, and one regarding the fatigue stepwise tests, where the two tested samples are denoted as UniPa and UniSal to indicate the different laboratories conducting the tests. Preliminary

tensile tests were performed to characterise the elastic and post-elastic behaviour of the material. Stress–strain curves from two nominally identical samples are shown in Figure 2. In one of the two tensile tests, the testing machine stopped before reaching the sample's final failure, due to a too conservative interlock set on displacement. It is evident that the two curves from the two samples nearly overlap, indicating good reproducibility of the material behaviour. Figure 1 shows photos of the two tensile samples after the test.

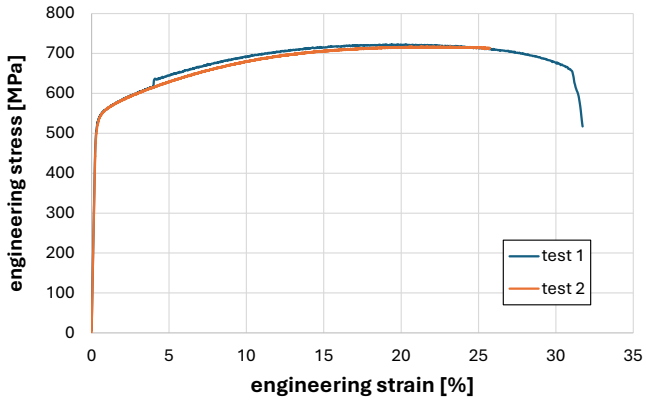

Figure 2. Tensile (σ, ϵ) curves from two samples of the same batch.

3.1. Static Thermographic Method

Tensile tests were monitored by an IR camera (cooled sensor FLIR X6540sc), measuring the surface temperature variation during the first elastic and initial post-elastic stages. The temperature evolution plotted in Figure 3 is the average temperature measured from a region of interest located over the sample central gauge area. The curve exhibits the three canonical phases of the STM [8,29]: (i) linear thermoelastic cooling; (ii) a deviation from linearity associated with the onset of micro-damage; and (iii) a subsequent rise approaching yielding. Consistent with the theoretical framework, segment (i) is governed by the Kelvin thermoelastic term, whereas the ensuing deviation reflects the emergence of non-negligible inelastic dissipation.

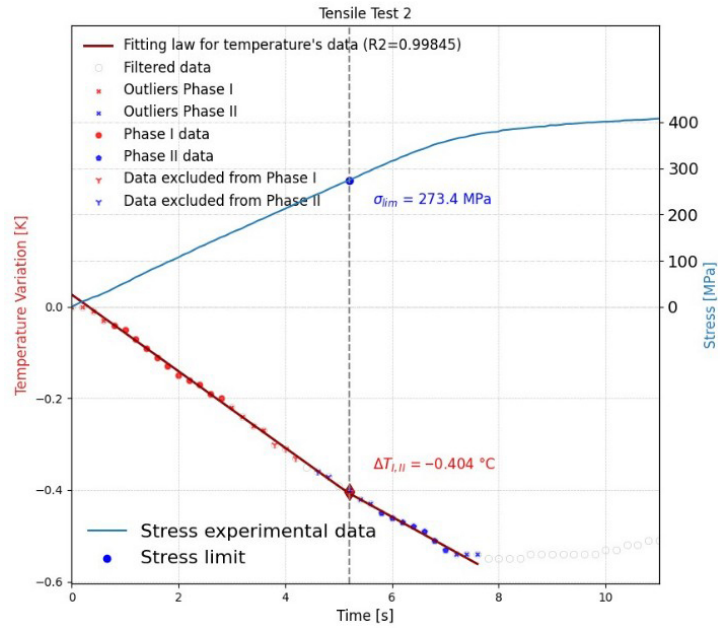

Figure 3. Static thermographic method (STM).

The datasets used for regression were cleaned with an adaptive-threshold *IQR* (Interquartile Range) filter; excluding ∼10% at the end of Phase I and ∼20% at the beginning of Phase II follows best-practice recommendations to mitigate bias around the slope-change region by fitting in less noisy portions [29]. When this procedure is applied to the $\Delta T(t)$ series in the figure, segment (i) is accurately linear ($R^2 \approx 0.9985$ on the selected subset), indicating a purely thermoelastic regime within the considered window. The intersection of the two regressions estimated after IQR filtering and local exclusions coincides with the instant marked by the vertical line; projection onto $\sigma(t)$ yields $\sigma_{\text{lim}} \approx 273.4$ MPa, to be interpreted as the STM *limit stress* (inception of macroscopic damage) for the quasi-static test performed. The annotation $\Delta T_{r,\text{II}} \approx -0.404\,^{\circ}\text{C}$ at the end of segment (ii) indicates that the dissipative contribution remains limited in the vicinity of t_{int}, consistent with damage initiation rather than fully developed yielding. The resulting σ_{lim} is then assumed to represent a threshold at which the dissipative component of the thermal balance becomes measurable with respect to thermoelastic cooling, under monotonic loading.

3.2. Fatigue Stepwise Method

The UniPa sample was instrumented with an extensometer during stepwise fatigue carried out according to Table 1. Figure 4 reports the first stabilised hysteresis cycle for each step. The average sample strain significantly increases to values around 13.5%, also for cyclic steps below the yield. Even so, all cycles up to failure maintained a rather small hysteresis area, which is only slightly increased during the last step acquisition after around 27,000 cycles.

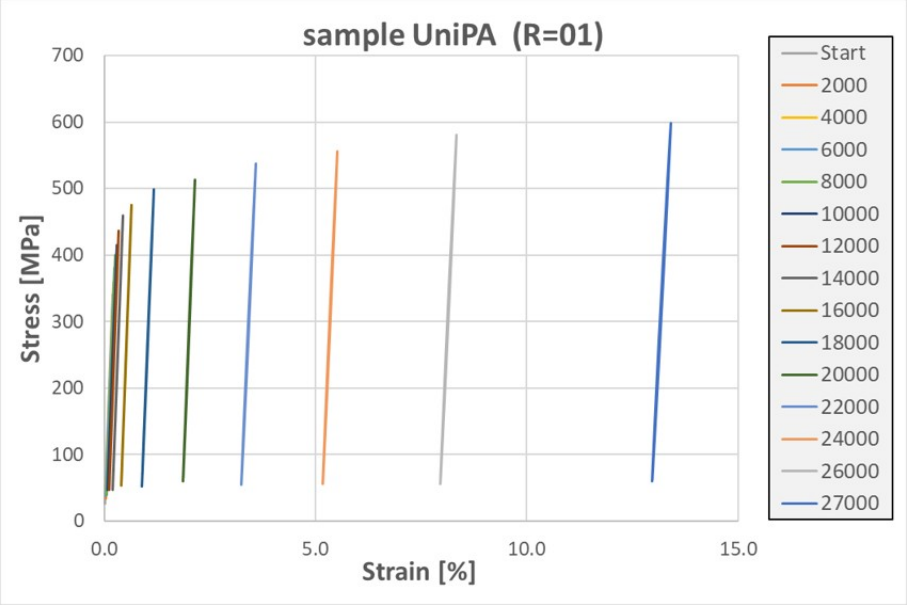

Figure 4. Hysteresis cycles.

It is useful to report that the black paint applied to enhance and make the infrared emissivity uniform started to de-bond in the UniPa sample as this reached higher stress amplitudes (Figure 5). This severely disturbed the harmonic metrics measurement. The UniSal sample did not experience the same issue, and the paint remained attached to the sample up to final brake failure.

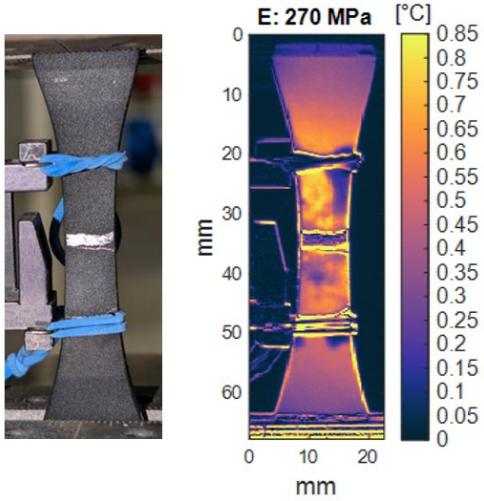

Figure 5. Image of the UniPa tensile sample in the last step of cyclic loading ($\sigma = 270$ MPa), before failure. The map on the right shows the thermoelastic signal E.

Figure 6 shows the trend of the four harmonic metrics E, D, PhE, and PhD measured during the UniPa stepwise test. The same figure reports a map of E obtained from the 12th step acquisition (i.e., at $\sigma_a = 252$ MPa), where it is also shows the ROI area where the harmonic metrics are averaged and then plotted in the graphs reported aside. In particular, each plot reports two curves, one obtained from data acquired in a first acquisition window after 1000 cycles from the step cycling start and the second after 1800 cycles. Figure 7 reports analogous information from the UniSal test, where only one sampling window per step was acquired. Figure 8 reports a comparison between the results of the UniPa and UniSal stepwise metrics, where the plots of E, D, and PhE are reported together with the plot of the stabilised temperature change ΔT. In particular, when a loading step is completed (lasting 2000 and 3000 cycles in the UniPa and UniSal tests, respectively), the applied mean load remains constant for 30 s before adjusting to the values of the next load step and triggering the next cyclic loading. The stabilised ΔT values in Figure 8 are calculated by averaging the temperature over the last 500 cycles of each load step and subtracting the averaged temperature from the first load step. This can be considered equivalent to applying the classic stabilised-plateau Risitano Method (RM) [8].

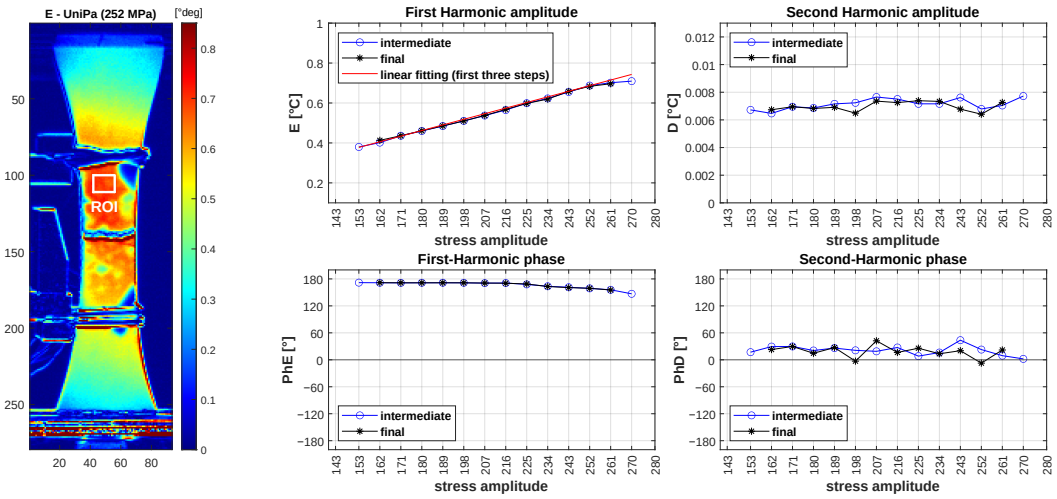

Figure 6. Stepwise harmonic metrics analysis from UniPa. The plot on the left-hand side shows a map of E and the location of the ROI where the harmonic metrics are averaged and plotted on the graphs in the right-hand side.

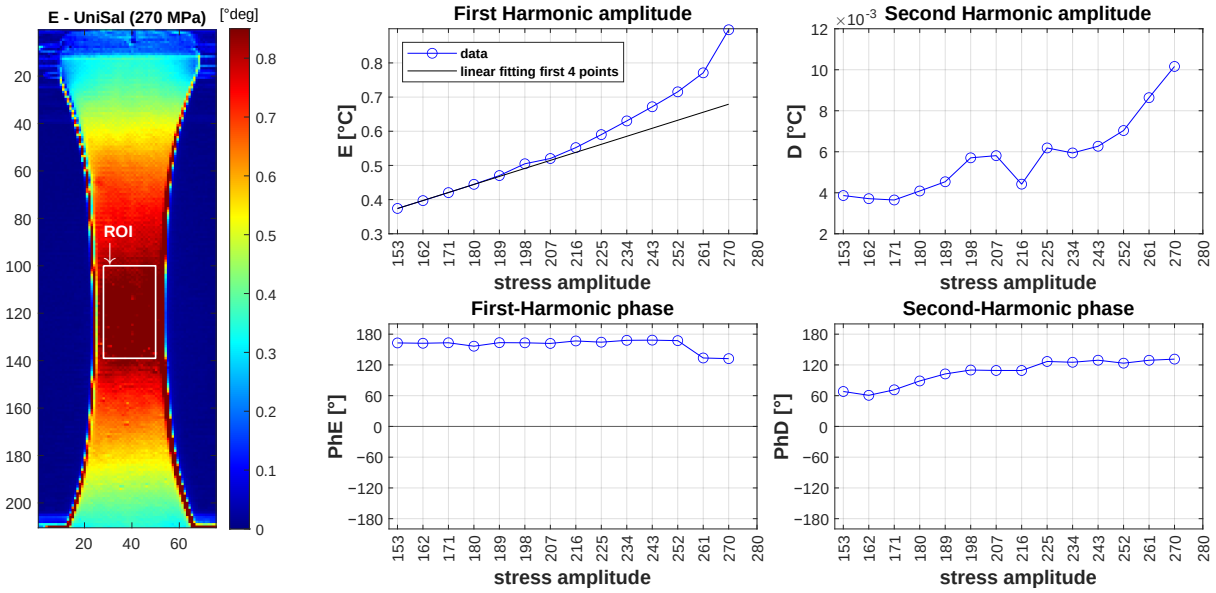

Figure 7. Stepwise harmonic metrics analysis from UniSal. The plot on the left-hand side shows a map of E from the 14th step, and the location of the ROI where the harmonic metrics are averaged and plotted on the graphs in the right-hand side.

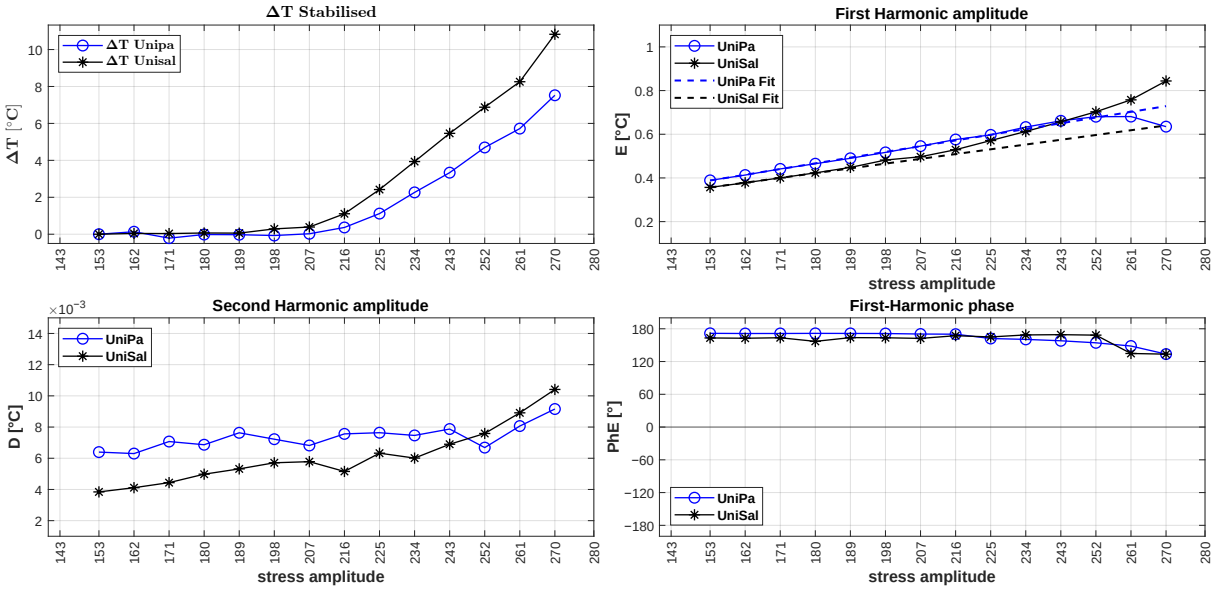

Figure 8. Comparison between UniPa and UniSal stepwise metrics results.

Figures 9 and 10 report the values from of the second-harmonic phase angle *PhD* in terms of occurrences over a central gauge area of the sample. It is noted that the values appear to be variously distributed over the range from −180° to 180°. It is useful to remember here that the second-harmonic term predicted by the second-order thermoelastic theory (see Section 2.1) would expect the *PhD* values to concentrate around the position of either 180° or −180°, while a dissipative second-harmonic behaviour would collocate *PhD* around 0°.

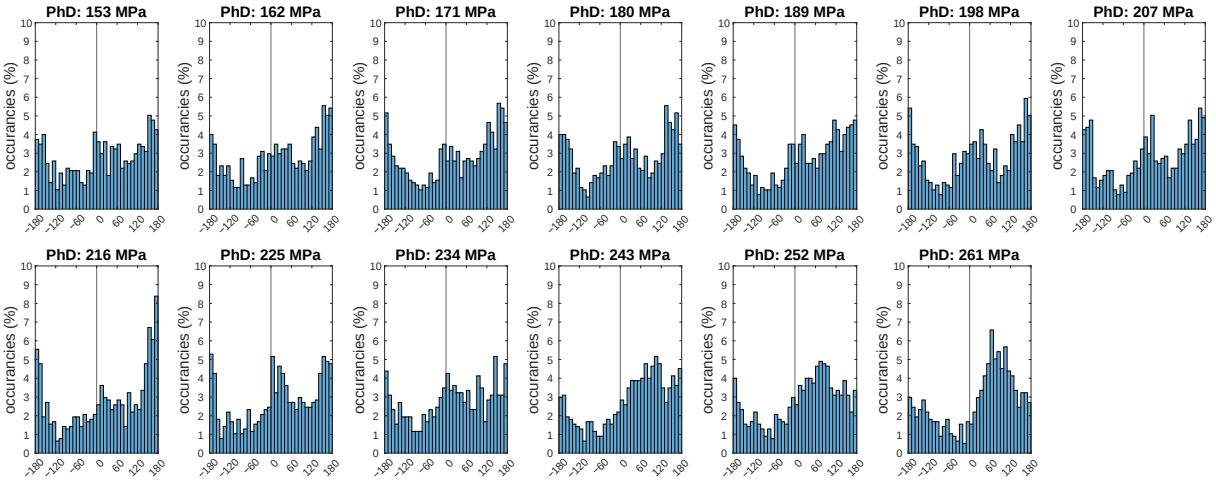

Figure 9. Histograms of second-harmonic phase angle distribution from each pixel in the monitored ROI: UniPa tests.

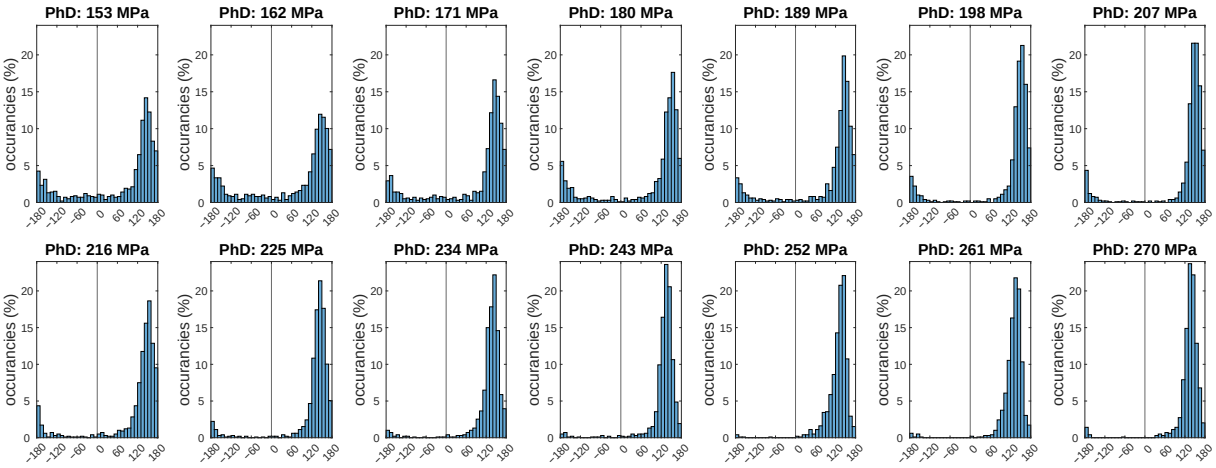

Figure 10. Histograms of second-harmonic phase angle distribution from each pixel in the monitored ROI: UniSal tests.

4. Discussion

Among the FLMT techniques implemented in this work, perhaps the ones that more clearly seem to identify a threshold stress of dissipation onset are the STM and the RM (see the ΔT plot in the first row, first column of Figure 8). The STM, though, yields a higher threshold stress value of $\sigma_{t_h} = 273$ MPa, while the RM yields a value between 207 and 216 MPa. This could be due to a different influence of the applied average stress in the monotonic tensile test compared to the $R = 0.1$ loading ratio of stepwise tests. Regarding the harmonic methods, the results are more ambiguous and difficult to interpret. The problem of the detachment of the coating in the UniPa test could be one reason for the discrepancies with the UniSal results. From the UniPa results, it is noted that a near identical outcome is found between the data acquired at 1000 and 1800 step cycles. The trend of E from the UniPa tests is very much linear up to the last two steps, when the detaching coating begins to become quite severe and spread (see Figure 5). It must be said that the linear trend is the one expected from the thermoelastic first-order law, when no significant deviation due to heat dissipation intervenes. Having said that, the UniSal trend of E is instead showing a deviation from linearity after about 207 MPa (in agreement with the RM value). The trend of PhE from the UniPa tests seems to show a slight deviation from the 180° value after 207 MPa, which could again be interpreted as a sign that the coating is starting to detach at this stress value. On the contrary, the UniSal trend of PhE

does not seem to show any meaningful deviations around 207 MPa. Remember that the 180° value is the angle expected if the first harmonic is mainly thermoelastic.

The second-harmonic amplitude D from UniPa (Figure 6) does not reveal any appreciable trend throughout the σ_a steps, up to final fracture. This limited sensitivity, together with the rather small values, might indicate that the harmonic is very close to the noise floor of the filtering techniques. A potential confirmation of this comes from analysing the occurrence values of PhD from Figure 9. The values of PhD are not seen to converge at specific angles and are scattered quite randomly throughout the range of −180° to 180°. This can be explained by the influence of random noise and the possibility that the second harmonic remains embedded below the noise floor [23]. The UniSal d and PhD results, on the other hand, seem to identify more deterministic outcomes. In particular, D is observed to exhibit an increasing trend at approximately 207 MPa. The histograms of the PhD distribution in Figure 10 show a peculiar concentration of values around 100°. This angle cannot be associated with either a dissipative or thermoelastic behaviour, which might suggest that in this case, there could be some important spurious second-harmonic component in the load signal [25]. It is finally added that fatigue failure in both UniPa and UniSal tests occurred in a sudden and brittle manner, with no evidence of macro-crack formation and stable crack propagation. Post-mortem observations revealed a marked presence of porosity and pitting, defects inherently associated with the additive manufacturing process (see also the zoomed particular shown in Figure 1). These discontinuities likely acted as stress concentrators, accelerating the enucleation of small cracks and lowering the critical stress for fracture.

5. Conclusions

This study presents preliminary findings from an ongoing experimental campaign investigating the use of accelerated Fatigue Limit Thermographic Methods (FLTMs) to identify intrinsic fatigue limits in LPBF-manufactured steel. Traditional FLTM techniques (STM and RM) and temperature harmonic analysis have been applied through stepwise fatigue loading tests with load ratio R = 0.1. The initial results suggest the presence of a threshold stress amplitude associated with the onset of heat dissipation. Although further validation is needed, the presented setup and methodology establish a foundation for future studies to investigate the fatigue behaviour and failure mechanisms of AM metals.

Author Contributions: Conceptualisation, G.P., G.R. and F.W.P.; methodology, G.P., G.R. and F.W.P.; software, G.P., G.R., D.D. and M.T.; validation, M.T., G.P., D.D., G.R., R.P. and F.W.P.; resources, F.W.P., G.P. and G.R.; data curation, M.T., D.D., R.P. and G.P.; writing—original draft preparation, G.P. and M.T.; writing—review and editing, M.T., G.P., G.R. and F.W.P.; visualisation, M.T. and G.P.; supervision, F.W.P., G.P. and G.R.; project administration, F.W.P., G.P. and G.R.; funding acquisition, F.W.P., G.P. and G.R. All authors have read and agreed to the published version of the manuscript.

Funding: The present research has received funding from the European Union's Framework Program for Research and Innovation-Mission 4-Component C2 Investment 1.1 (PRIN-2022)—project title MADforLIFE, code: 2022JE3LRA-001, CUP: B53D23006070006.

Institutional Review Board Statement: Not applicable.

Informed Consent Statement: Not applicable.

Data Availability Statement: All raw data that support the findings of this study are available from the corresponding author, upon reasonable request.

Acknowledgments: The authors thank MadeInAdd SRL (https://www.madeinadd.com, accessed on 1 March 2026) for the advice and assistance with the manufacturing of the tested samples.

Conflicts of Interest: The authors declare no conflicts of interest.

Abbreviations

The following abbreviations are used in this manuscript:

AM	Additive manufacturing
DMLS	Direct Metal Laser Sintering
FLMT	Fatigue Limit Thermographic Method
LF	Load frequency
LPBF	Laser-based Powder Bed Fusion
IQR	Inter-quartile Range
RM	Risitano's method
SF	Sampling frequency
STM	Static Thermographic Method
TH	Temperature harmonics
TSA	Thermoelastic stress analysis

References

1. Karakurt, I.; Lin, L. 3D printing technologies: Techniques, materials, and post-processing. *Curr. Opin. Chem. Eng.* **2020**, *28*, 134–143. [CrossRef]
2. D'Andrea, D. Additive Manufacturing of AISI 316L Stainless Steel: A Review. *Metals* **2023**, *13*, 1370. [CrossRef]
3. Wei, W.; He, L.; Sun, Y.; Yang, X. A Review of Fatigue Limit Assessment Using the Thermography-Based Method. *Metals* **2024**, *14*, 640. [CrossRef]
4. Teng, Z. Thermo-based fatigue life prediction: A review. *Fatigue Fract. Eng. Mater. Struct.* **2023**, *46*, 3121–3144. [CrossRef]
5. Zaeimi, M.; De Finis, R.; Palumbo, D.; Galietti, U. Fatigue limit estimation of metals based on the thermographic methods: A comprehensive review. *Fatigue Fract. Eng. Mater. Struct.* **2024**, *47*, 611–646. [CrossRef]
6. Chapetti, M.D.; Gubeljak, N.; Kozak, D. Intrinsic Fatigue Limit and the Minimum Fatigue Crack Growth Threshold. *Materials* **2023**, *16*, 5874. [CrossRef]
7. Madia, M.; Zerbst, U.; Werner, T. Estimation of the Kitagawa-Takahashi diagram by cyclic R curve analysis. *Procedia Struct. Integr.* **2022**, *38*, 309–316. [CrossRef]
8. Santonocito, D.; Fintová, S.; Di Cocco, V.; Iacoviello, F.; Risitano, G.; D'Andrea, D. Comparison on mechanical behavior and microstructural features between traditional and AM AISI 316L. *Fatigue Fract. Eng. Mater. Struct.* **2023**, *46*, 379–395. [CrossRef]
9. Crisafulli, D.; Fintová, S.; Santonocito, D.; D'Andrea, D. Microstructural characterization and mechanical behaviour of laser powder Bed Fusion stainless steel 316L. *Theor. Appl. Fract. Mech.* **2024**, *131*, 104343. [CrossRef]
10. Santoro, L.; Sesana, R.; Diller, J.; Radlbeck, C.; Mensinger, M. Dissipative and thermal aspects in cyclic loading of additive manufactured AISI 316L. *Eng. Fail. Anal.* **2024**, *163*, 108446. [CrossRef]
11. Zhang, H.; Li, C.; Song, W.; He, N.; Wang, F.; Zhang, Y. Fatigue life evaluation and cellular substructure role of laser powder bed fused 304L steel based on dissipative deformation mechanisms. *Addit. Manuf.* **2023**, *64*, 103430. [CrossRef]
12. Matušů, M.; Šimota, J.; Papuga, J.; Rosenthal, J.; Beránek, L.; Costa, P.; Bumba, F.; Reis, L. S–N curves established from limiting energy in the case of specimens additively manufactured from AlSi10Mg. *Fatigue Fract. Eng. Mater. Struct.* **2024**, *47*, 4771–4790. [CrossRef]
13. Matušů, M.; Džuberová, L.; Papuga, J.; Rosenthal, J.; Šimota, J.; Beránek, L. Fatigue analysis and heat treatment comparison of additively manufactured specimens from AlSi10Mg alloy. *Int. J. Fatigue* **2024**, *185*, 108357. [CrossRef]
14. Colombo, C.; Tridello, A.; Pagnoncelli, A.P.; Biffi, C.A.; Fiocchi, J.; Tuissi, A.; Vergani, L.M.; Paolino, D.S. Efficient experimental methods for rapid fatigue life estimation of additive manufactured elements. *Int. J. Fatigue* **2023**, *167*, 107345. [CrossRef]
15. Pathak, P.; Gururaja, S.; Kumar, V.; Nuttall, D.; Mahmoudi, A.; Khonsari, M.; Vaidya, U. Examining infrared thermography based approaches to rapid fatigue characterization of additively manufactured compression molded short fiber thermoplastic composites. *Compos. Struct.* **2025**, *351*, 118610. [CrossRef]
16. Bercelli, L.; Doudard, C.; Calloch, S.; Le Saux, V.; Beaudet, J. Thermometric investigations for the characterization of fatigue crack initiation and propagation in Wire and Arc Additively Manufactured parts with as-built surfaces. *Fatigue Fract. Eng. Mater. Struct.* **2023**, *46*, 153–170. [CrossRef]
17. De Finis, R.; Palumbo, D.; Ancona, F.; Galietti, U. Fatigue limit evaluation of various martensitic stainless steels with new robust thermographic data analysis. *Int. J. Fatigue* **2015**, *74*, 88–96. [CrossRef]
18. Cappello, R.; Meneghetti, G.; Ricotta, M.; Pitarresi, G. On the correlation of temperature harmonic content with energy dissipation in C45 steel samples under fatigue loading. *Mech. Mater.* **2022**, *168*, 104271. [CrossRef]

19. Palumbo, D.; Galietti, U. Thermoelastic Phase Analysis (TPA): A new method for fatigue behaviour analysis of steels. *Fatigue Fract. Eng. Mater. Struct.* **2017**, *40*, 523–534. [CrossRef]
20. Colombo, C.; Sansone, M.; Patriarca, L.; Vergani, L. Rapid estimation of fatigue limit for C45 steel by thermography and digital image correlation. *J. Strain Anal. Eng. Des.* **2021**, *56*, 478–491. [CrossRef]
21. Meneghetti, G.; Ricotta, M. Estimating the intrinsic dissipation using the second harmonic of the temperature signal in tension-compression fatigue: Part I. Theory. *Fatigue Fract. Eng. Mater. Struct.* **2021**, *44*, 2168–2185. [CrossRef]
22. Wong, A.; Jones, R.; Sparrow, J. Thermoelastic constant or thermoelastic parameter? *J. Phys. Chem. Solids* **1987**, *48*, 749–753. [CrossRef]
23. Pitarresi, G.; Cappello, R.; Catalanotti, G. Quantitative thermoelastic stress analysis by means of low-cost setups. *Opt. Lasers Eng.* **2020**, *134*, 106158. [CrossRef]
24. De Finis, R.; Palumbo, D.; Galietti, U. A multianalysis thermography-based approach for fatigue and damage investigations of ASTM A182 F6NM steel at two stress ratios. *Fatigue Fract. Eng. Mater. Struct.* **2019**, *42*, 267–283. [CrossRef]
25. Cappello, R.; Semedo Garção, J.E.; Catalanotti, G.; Pitarresi, G. On the Identification of Dissipative Phenomena in Fatigue-Loaded 2024 Aluminum by Means of Second Harmonic of Temperature Analysis. *Fatigue Fract. Eng. Mater. Struct.* **2025**, *48*, 4105–4118. [CrossRef]
26. Enke, N.F. An enhanced theory for thermographic stress analysis of isotropic materials. In *Proceedings of the Stress and Vibration: Recent Developments in Industrial Measurement and Analysis*; International Society for Optics and Photonics: Bellingham, Washington, USA, 1989; Volume 1084, pp. 84–102.
27. Krapez, J.; Pacou, D.; Gardette, G. Lock-in thermography and fatigue limit of metals. *Quant. Infrared Thermogr.* **2000**, *5*, 277–282. [CrossRef]
28. *ASTM E466-21*; Standard Practice for Conducting Force Controlled Constant Amplitude Axial Fatigue Tests of Metallic Materials. ASTM International: West Conshohocken, PA, USA, 2021.
29. D'Andrea, D.; D'Andrea, D.; Risitano, G.; Santonocito, D. Advanced algorithms for early detection of first damage during static tensile tests. *Fract. Struct. Integr.* **2025**, *19*, 294–309. [CrossRef]